The Astrophysical Journal, 946:31 (14pp), 2023 March 20 https://doi.org/10.3847/1538-4357/acbfa8


# Searching for Supernovae in HETDEX Data Release 3*

József Vinkó[1,2,3,4], Benjamin P. Thomas[1], J. Craig Wheeler[1], Anna Y. Q. Ho[5], Erin Mentuch Cooper[1], Karl Gebhardt[1], Robin Ciardullo[6,7], Daniel J. Farrow[8,9], Gary J. Hill[1,10], Zoltán Jäger[11,12,13], Wolfram Kollatschny[14], Chenxu Liu[1,15], Enikő Regős[2], and Krisztián Sárneczky[2]

[1] Department of Astronomy, University of Texas at Austin, 2515 Speedway, Stop C1400 Austin, Texas 78712-1205, USA; vinko@konkoly.hu
[2] Konkoly Observatory, CSFK, Konkoly-Thege M. út 15-17, Budapest, 1121, Hungary
[3] ELTE Eötvös Loránd University, Institute of Physics, Pázmány Péter sétány 1/A, Budapest, 1117 Hungary
[4] Department of Experimental Physics, University of Szeged, Dóm tér 9, Szeged, 6720, Hungary
[5] Department of Astronomy, Cornell University, Ithaca, NY 14853, USA
[6] Department of Astronomy & Astrophysics, The Pennsylvania State University, University Park, PA 16802, USA
[7] Institute for Gravitation and the Cosmos, The Pennsylvania State University, University Park, PA 16802, USA
[8] University Observatory, Fakultät für Physik, Ludwig-Maximilians University Munich, Scheinerstrasse 1, D-81679 Munich, Germany
[9] Max-Planck Institut für Extraterrestrische Physik, Giessenbachstrasse 1, D-85748 Garching, Germany
[10] McDonald Observatory, The University of Texas at Austin, 2515 Speedway, Stop 1402, Austin, TX 78712, USA
[11] Baja Observatory, University of Szeged, Szegedi út POB 766, Baja, 7900, Hungary
[12] ELTE Eötvös Loránd University, Gothard Astrophysical Observatory, Szent Imre h.u. 112, Szombathely, 9700, Hungary
[13] MTA-ELTE Exoplanet Research Group, Szent Imre h.u. 112, Szombathely, 9700, Hungary
[14] Institut für Astrophysik, Universität Göttingen, Friedrich-Hund Platz 1, D-37077 Göttingen, Germany
[15] South-Western Institute for Astronomy Research, Yunnan University, Kunming, Yunnan, 650500, People's Republic of China
*Received 2022 August 25; revised 2023 February 7; accepted 2023 February 20; published 2023 March 24*

## Abstract

We have extracted 636 spectra taken at the positions of 583 transient sources from the third data release of the Hobby–Eberly Telescope Dark Energy eXperiment (HETDEX). The transients were discovered by the Zwicky Transient Facility (ZTF) during 2018–2022. The HETDEX spectra provide a potential means to obtain classifications for a large number of objects found by photometric surveys for free. We attempt to explore and classify the spectra by utilizing several template-matching techniques. We have identified two transient sources, ZTF20aatpoos = AT 2020fiz and ZTF19abdkelq, as supernova (SN) candidates. We classify AT 2020fiz as a Type IIP SN observed ∼10 days after explosion, and we propose ZTF19abdkelq as a likely Type Ia SN caught ∼40 days after maximum light. ZTF photometry of these two sources are consistent with their classifications as SNe. Beside these two objects, we have confirmed several ZTF transients as variable active galactic nuclei based on their spectral appearance, and determined the host galaxy types of several other ZTF transients.

*Unified Astronomy Thesaurus concepts:* SNe (1668); Active galactic nuclei (16); Spectroscopy (1558)

*Supporting material:* machine-readable tables

## 1. Introduction

The advent of deep, all-sky, untargeted surveys, such as the Zwicky Transient Facility (ZTF; Bellm et al. 2019), the Dark Energy Survey (DES; Bernstein et al. 2012; Kessler et al. 2015) and the upcoming Vera Rubin Telescope Legacy Survey in Space and Time (LSST; Ivezić et al. 2019) have ushered in a new age for the study of transient astronomy, and it is now one of the most popular fields in astronomy and astrophysics. The thousands of new transients discovered each day offer the potential to build statistical samples of otherwise rare and poorly known phenomena, such as tidal disruption events (Gezari 2021) and superluminous supernovae (SNe; Gal-Yam 2019), as well as find new types of transient objects that are either rare (like kilonovae) or currently remain unknown.

SNe are among the most well known and frequently studied transient objects for several reasons. First, due to their outstanding peak brightness, they can be discovered and studied even at high redshifts, i.e., $z > 1$. Moreover, the ∼month timescale of their evolution is neither too fast nor too slow compared to human timescales, which makes them ideal targets for astrophysical studies. Also, SNe are among the best distance indicators in extragalactic astronomy, and thus, are useful from not only an astrophysical, but also a cosmological point of view; for example, the discovery of the accelerated expansion of the universe was at first based on distance measurements from Type Ia SNe (Riess et al. 1998; Perlmutter et al. 1999). Finally, the James Webb Space Telescope (JWST) and future space observatories will extend our cosmic horizon considerably, thus, enabling the discovery of transients beyond $z > 2$, in the very early universe (e.g., Regős & Vinkó 2019; Regős et al. 2020, 2021). The recently discovered very-high-redshift galaxies at $z > 12$—including one at $z = 16.7$—by JWST (Donnan et al. 2022) improve our understanding of the cosmic star formation rate at $z > 8$ and the epoch of reionization. Studies of these high-redshift SNe will ultimately constrain the (true) initial mass function of the first stars.

The unprecedented number of new transients in the data stream makes their analysis very challenging. Since spectroscopy is "expensive" in terms of telescope time, most of the surveys

* Based on observations obtained with the Hobby–Eberly Telescope (HET), which is a joint project of the University of Texas at Austin, the Pennsylvania State University, Ludwig-Maximillians-Universitaet Muenchen, and Georg-August Universitaet Goettingen. The HET is named in honor of its principal benefactors, William P. Hobby and Robert E. Eberly.

mentioned above are based on imaging and photometry. Thus, the possibility for a prompt revealing of the physical nature of new transients is limited. As most classification schemes require (mostly optical) spectroscopy, it is not currently possible to definitively classify the bulk of these new sources. Instead, the current strategy is concentrated on identifying potentially interesting sources based on either their position (e.g., being in a nearby galaxy or galaxy cluster) or their photometric properties (e.g., unusually bright, blue/red, fast/slow evolution, etc.). This still leaves most transients unclassified and they fade away with minimal spectroscopic attention.

In such circumstances, survey programs that produce a massive number of spectroscopic observations can be useful. One of them is the Hobby–Eberly Telescope Dark Energy eXperiement (HETDEX; Gebhardt et al. 2021; Hill et al. 2021). HETDEX is a blind spectroscopic survey that, once completed, will use observations of 1.2 million Ly$\alpha$ emitting galaxies to measure baryonic acoustic oscillations (BAOs) and constrain the fundamental parameters that describe the time evolution of the dark energy equation of state. HETDEX aims to obtain spectral coverage of 540 deg$^2$ of the sky with a filling factor of 1 in 4.6; a spectrum is obtained at every position that is covered by a fiber in the field of view, including all objects that are brighter than the HETDEX 5$\sigma$ limiting magnitude of $m_{\rm lim}({\rm AB}) \sim 22.5$ in the $g$ band (Gebhardt et al. 2021).

The HETDEX survey is unique as it contains untargeted, deep, wide-field spectroscopic data. While HETDEX is at heart a high-redshift galaxy survey (Davis et al. 2021; Lujan Niemeyer et al. 2022), it also obtains spectra of all other objects in its field of view, including stars of all types (Hawkins et al. 2021), early- and late-type galaxies (Indahl et al. 2021), high-redshift quasars (Zhang et al. 2021; Liu et al. 2022), and, in principle, SNe. The unbiased nature of the HETDEX spectroscopic selection function implies that there must exist spectra of anomalous, perhaps unprecedented, objects within the HETDEX continuum-source catalog. The HETDEX data can also be used, at least potentially, for the classification of all types of transient objects that appear within the survey footprint.

Another advantage of HETDEX is that it uses integral field units (IFUs), thus, not only single objects but also their immediate environment can be observed spectroscopically. This could be promising, for example, for studying the hosts of extragalactic transients (see Section 4.6). Also, finding unbiased transient spectra that can be applied in training sets for machine learning (ML) methods could be a great by-product of the survey (e.g., Ishida et al. 2019).

In this paper we present the first attempt to use HETDEX data for spectroscopic classification and characterization of transients that were discovered within the survey's footprint. While our primary purpose was finding SNe, it turned out that the HETDEX spectra are also useful for identifying variable active galactic nuclei (AGNs), and studying the host galaxies of SNe and other transients.

This paper is organized as follows. Data extraction is outlined in Section 2, then the applied classification methods are detailed in Section 3. The results are discussed in Section 4, while the conclusions are summarized in Section 5.

## 2. Data

HETDEX uses the Visible Integral-field Replicable Unit Spectrograph (VIRUS; Hill et al. 2021) instrument at the focal surface of the HET (Ramsey et al. 1998; Hill et al. 2021). VIRUS comprises up to 78 IFUs, each with 448 1.″5-diameter fibers, such that 33,152 individual spectra covering 54 arcmin$^2$ are obtained with each visit. The spectra extend from 3500 to 5500 Å with a resolution of ∼2 Å. For more details about the survey design concepts and specifications, see Gebhardt et al. (2021). For more details about the instrumentation, see Hill et al. (2021).

The HETDEX Data Release 2.1 (HDR2.1) continuum-source catalog contains spectra for ∼62k unique objects (Mentuch Cooper et al. 2023), and includes a vast amount of information that is too large to be visually classified by human experts. Thus, the very nature of the HETDEX survey design motivates ML efforts not only for anomaly detection, but also for object classification. In the HETDEX Data Release 3 (HDR3), the size of the continuum-source catalog has been extended further, reaching ∼230k sources. In this paper we use the more extensive HDR3 data set.

SNe identifications in the HETDEX catalog are challenging, not least because they are not the ultimate target of the survey. As a result, the various reduction pipelines that produce the survey's data products are not optimized to find extragalactic transients. For example, one such issue is that, within the continuum-detection process, sources are rejected if they are within 1.″5 of another galaxy; in these cases only the brightest continuum object remains in the catalog. This cut may discard SNe and similar astronomical transients that are associated with a bright host galaxy, but are actually separate point sources near their host galaxy's core. We therefore opted not to use the default HETDEX data products for our initial search for SNe.

Instead, for this work we chose to perform forced spectral extractions at the known locations of transient sources. There are many astronomical surveys that can provide auxiliary information to HETDEX. One of these is ZTF (Bellm et al. 2019; Graham et al. 2019; Masci et al. 2019; Dekany et al. 2020), which covers the full northern sky in two filters every three nights. This survey typically produces between $10^5$ and $10^6$ alerts per night (Förster et al. 2021), 80% of which are associated with real astronomical sources (Carrasco-Davis et al. 2021). Thus, we aimed to extract spectra at the positions of public ZTF transients announced between 2017 and early 2022 from the HETDEX spectroscopic data set, in the hopes of finding SN-like signals (broad features) in those spectra (see also Fremling et al. 2020). Details are given in the rest of this paper.

### 2.1. Source Extraction

We used the Automatic Learning for the Rapid Classification of events (ALeRCe; Förster et al. 2021) application programming interface (API)[16] to query the ZTF servers to find all detected ZTF transients that were within 12′ of the position of an HETDEX pointing. (This is roughly the size of the HET's usable focal plane, which is 20′ in diameter.) We then determined which of the resulting 4585 ZTF sources fell within 3.″5 of any of the ∼34,000 fibers that are part of VIRUS. This additional downsampling resulted in 636 spectra of 583 objects matched between ZTF and HETDEX. (Although HETDEX is a single-epoch survey, some science verification fields have been observed multiple times.) Using `HETDEX-`

[16] https://alerce.readthedocs.io/en/latest/tutorials/ztf_api.html

API/get_spec.py,[17] we were then able to extract HETDEX spectra that are closely matched to each of these transient locations. We used a point-spread function (PSF)-weighted 1D extraction at the exact position that the ZTF source was detected and required that at least seven fibers be contained within the 3.″5 circular aperture that is needed to capture the VIRUS PSF fully. Thus, the final spectrum is produced from a PSF-weighted sum over many fibers combined within a circular aperture with a radius of 3.″5 (Gebhardt et al. 2021).

It is worth noting here that the HETDEX spectra associated with these sources may not have been taken while the prospective transient was active. Indeed, in the majority of cases (494 out of 636) they were not. We can, however, still search for the nebular spectra of SNe that have faded beyond the ZTF detection limit. While searches for preSN progenitor stars may also be possible, it is likely that those progenitors will be too faint for detection.

## 3. Methods

This section summarizes the various methods that we applied to explore and characterize the extracted HETDEX spectra.

### 3.1. Visualization: t-SNE

A large number of discoveries in astronomy, and science more generally, have been catalyzed due to some degree of serendipity. Visualization techniques may help the identification of the general trends as well as the peculiarities/outliers in massive amount of data.

One method that facilitates the visual exploration of large data sets is t-distributed stochastic neighbor embedding (t-SNE; van der Maaten & Hinton 2008). The t-SNE program is fundamentally a dimensionality-reduction technique that preserves the pairwise similarity between points while producing a $d$-dimensional map of those points (usually $d = 2$). We use the version of t-SNE implemented in the scikit-learn Python package (Pedregosa et al. 2011).

Here the dimensionality of the high-order space is set by the number of flux measurements (1036) in a single HETDEX spectrum. The t-SNE program works by first computing pairwise similarities $p_{ij}$ between these high-dimensional data points $x_i$ and $x_j$,

$$p_{j|i} = \frac{\exp(-||x_i - x_j||^2/2\sigma_i^2)}{\sum_{k\neq i}\exp(-||x_i - x_k||^2/2\sigma_i^2)}, \quad (1)$$

where $x_i$ is the $i$th HETDEX spectrum (representing a point in the 1036-dimensional space) and $\sigma_i$ is the variance of a Gaussian distribution centered on point $x_i$. This parameter is related to a user-defined hyperparameter called the perplexity. We choose a perplexity value of $\sqrt{N}$, where $N$ is our number of data points.

To reduce the effect of the presence of outliers, the symmetrical pairwise similarity is defined as,

$$p_{ij} = \frac{p_{j|i} + p_{i|j}}{2N}, \quad (2)$$

where $p_{j|i}$ is the probability that point $x_i$ would choose point $x_j$ as its nearest neighbor under the assumption of a Gaussian probability distribution centered at point $x_i$.

The next step is for t-SNE to attempt to learn a low-dimensional ($d = 2$) representation of the points, $y_1,\ldots,y_N$, that preserves the high-dimensional similarities $p_{ij}$ as analogous low-dimensional similarities $q_{ij}$. In this low-dimensional map,

$$q_{ij} = \frac{(1 + ||y_i - y_j||^2)^{-1}}{\sum_{k\neq m}(1 + ||y_k - y_m||^2)^{-1}}. \quad (3)$$

This metric is related to the Student's t-distribution (e.g., Press et al. 2002), and its primary purpose is to avoid overcrowding in the low-dimensional embedded space. Also, the Student's t-distribution is faster to compute compared to a Gaussian as it does not contain any exponential terms.

The key process of t-SNE is to determine the low-dimensional embeddings of the points $y_i$ by minimizing (via gradient-descent) the Kullback–Leibler divergence between the low- and high-dimensional similarity distributions $P$ and $Q$,

$$\mathrm{KL}(P||Q) = \sum_{i\neq j} p_{ij}\log\frac{p_{ij}}{q_{ij}}. \quad (4)$$

This will result in an optimized $d =$ two-dimensional map that preserves the similarities of points from the high-dimensional distribution.[18]

### 3.2. Classification: Template Matching Via $\chi^2$ minimization

The traditional method for automated classification of astronomical objects is through comparisons with a list of template spectra using a mathematical criterion to judge the quality of matching; the classification then follows from the best-matched template. We employed this template-matching scheme using as templates the Pickles Stellar Spectral Flux Library (Pickles 1998) for stars and the Kinney synthetic spectra (Kinney et al. 1996) for galaxies. The former contains 131 stellar spectra covering the Harvard classes from O5 through M4 and the Morgan–Keenan luminosity classes from I to V; the latter includes spectra for 11 galaxies, including an elliptical (E), a lenticular (S0), three spirals (Sa, Sb, and Sc) and six star-bursting (SB1—SB6) systems. The star-forming templates are dominated by emission features of varying strength, while the elliptical and lenticular templates represent the spectra of most passive galaxies.

We adopted $\chi^2$ statistics for measuring the quality of the match between the observed spectrum and a template. The normalized $\chi^2$ function was defined as,

$$\chi^2_N = \frac{1}{N}\sum_{k=0}^{N}\frac{1}{\sigma_k^2}(f_c^{\mathrm{obs}}(\lambda_k) - f_c^{\mathrm{templ}}(\lambda_k))^2, \quad (5)$$

where $N$ is the number of sampled wavelengths in an observed spectrum, the functions $f_c^{\mathrm{obs}}$ and $f_c^{\mathrm{templ}}$ are the continuum-normalized flux of the object and the template as a function of wavelength ($\lambda$), respectively, and $\sigma_k$ contains the uncertainties of the observed fluxes.

[17] https://github.com/HETDEX/hetdex_api/blob/master/hetdex_tools/get_spec.py

[18] Some other studies have used a principle component analysis to reduce the dimensionality of the data before feeding them into t-SNE. We found that this was not necessary in our case due to the relatively small size of the data set.

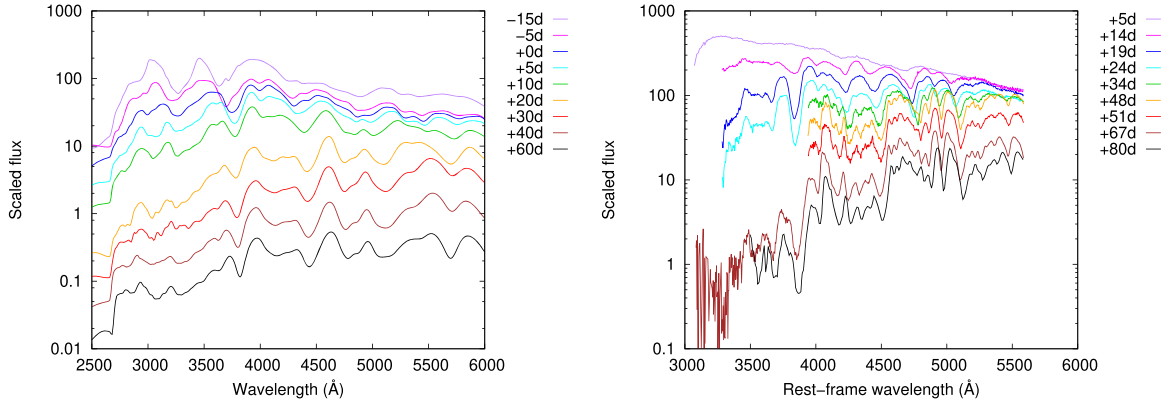


**Figure 1.** The series of SN spectral templates for SNe Ia (left) and SNe IIP (right) applied in the CCF method. The spectral phase in days for each template is indicated in the legend.

Before applying Equation (5), simple linear interpolation was applied to the template spectra to correct for the different wavelength sampling between the template and the observed spectra. In addition, both spectra were normalized to the continuum by iteratively fitting an eighth-order polynomial to both the observed and the template spectra. After each iteration, the standard deviation (`stddev`) of the residuals was calculated and data that exceeded the residuals by `-2×stddev` and `+3×stddev` were rejected from the sample. After ∼10 such iterations the fitted polynomial was found to represent the continuum reasonably well.

The uncertainties of the observed fluxes were estimated empirically by calculating the mean ($\langle f_c \rangle$) and standard deviation ($\sigma$) of the continuum-normalized data. In order to reduce the bias due to the presence of strong spectral features in the blue part of the spectra we used only the red part, between 4600 and 5400 Å, for this purpose. The same region was used to derive an empirical signal-to-noise ratio (S/N) parameter, defined as $\mathtt{s/n} = \langle f_c \rangle / \sigma$. Because of the presence of spectral features in the fitted wavelength region, this method clearly overestimates the noise in the case of spectra with moderate to high S/Ns, while giving more realistic results for noise-dominated data. We chose this simple approach of adopting a single $\sigma$ for the whole spectrum in Equation (5), i.e., $\sigma_k = \sigma$ for all $k$, because the majority of our sources did not reach high S/Ns, and the $\chi^2_N$ function was used only for measuring the quality of fitting between the observed and the template spectra. We do not treat the value as a proper statistical quantity.

Note that, as written, Equation (5) does not contain any terms for the possible redshift mismatch between the observed and the template spectra, and thus is only applicable for Milky Way objects with $z = 0$. Before using the equation for galaxies, the templates were therefore redshifted, and a value of $\chi^2_N$ was computed for each $z$ between $0 < z < 0.3$ range, using $dz = 0.001$ (see Section 4.2 for further information).

### 3.3. Classification: Template Matching Via Cross-correlation

The other widely used algorithm for template matching is cross-correlation. A code that is based on cross-correlation and applied very often in the SN community is Supernova Identification (`SNID`; Blondin & Tonry 2007), which uses the observed spectra of different types of SNe as templates. Such codes compute the cross-correlation function (CCF) between the observed ($f(\lambda)$) and the template ($g(\lambda)$) spectra via the following definition,

$$\mathrm{CCF}(\Delta x) = \int_{-\infty}^{+\infty} f(x) \cdot g(x - \Delta x) dx, \qquad (6)$$

where $x = \ln \lambda$, $\Delta x = \ln(\lambda/\lambda_0) = \ln(1 + z)$, $z$ is the redshift of the object. In short, the CCF measures the overlap, i.e., the similarity, between the object and the template spectra: the stronger the overlap, the greater the similarity of the two spectra. Thus, the height of the CCF peak is proportional to the overlap, while the horizontal shift ($\Delta x$) gives the redshift of the observed spectrum with respect to the template.

Because the public template libraries of `SNID` are based on published observed spectra, Type Ia SNe are overrepresented in them. In addition, most of these template libraries do not fully cover the HETDEX wavelength range of 3500–5500 Å. Thus, instead of applying `SNID` for our sample, we developed our own pipeline based on the `fxcor` task in `IRAF`.[19]

Since our primary intention was finding SNe, first, we adopted the Type Ia SN templates compiled by Eric Hsiao (Hsiao et al. 2007) for our analysis. These spectra span from −15 days to +91 days in phase with respect to the moment of $B$-band maximum, with a one day cadence. Since our single-epoch data do not allow precise temporal resolution, we preselected nine spectra from the library (having epochs at −15, −5, 0, +5, +10, +20, +30, +40, and +60 days with respect to maximum light) and used only those data in the cross-correlation. The selected SN Ia templates are shown in the left panel of Figure 1. Each template spectrum has $\Delta\lambda = 10$ Å resolution (which is much lower than the ∼2 Å resolution of the HETDEX spectra) and covers the wavelength interval between 2500 and 6000 Å.

Because the spectra of hydrogen-poor (Type Ib/c) core-collapse SNe are often similar to those of Type Ia SNe, at least around maximum light when the SN appears to be the brightest, we did not define a separate set of templates for those objects. Instead, the Hsiao templates were utilized for the SN Ib/c-type objects.

Second, for hydrogen-rich (Type II) core-collapse SNe, we adopted the published spectra of the archetypal Type IIP SN

[19] IRAF was distributed by the National Optical Astronomy Observatory, which is operated by the Association of Universities for Research in Astronomy (AURA) under a cooperative agreement with the National Science Foundation.

1999em (Hamuy et al. 2001; Elmhamdi et al. 2003), downloaded from the Weizmann Interactive SN Data Repository (WiseRep).[20] The selected spectra are corrected for the redshift of SN 1999em ($z = 0.002392$) and shown in the right panel of Figure 1. We chose only the spectra that were taken during the plateau phase (lasting ~100 days after the explosion), because the SN is brighter by at least 1.5–2 mag during this period than in the subsequent tail and nebular phase. Thus, it is more probable to detect a Type II at this time.

## 4. Results and Discussion

The results of our analysis are presented and discussed in this section.

### 4.1. Visualization with t-SNE

After having extracted spectra from the HETDEX database at the positions of the known ZTF transients (see Section 2.1), we normalized the spectra by their uncertainties (produced by the HETDEX reduction pipeline) to account for edge defects and other minor issues, and fed them directly into the t-SNE algorithm. This resulted in the two-dimensional map shown in Figure 2, which we could then explore and visually inspect. We created a point-and-click tool to examine the spectra represented by each t-SNE data point quickly and efficiently, and by this visual inspection process, we identified the clusters that were predominantly AGNs, star-forming galaxies, and low-S/N sources. We also flagged several objects that seemed to show broad spectral features, like SNe, for further analysis. These objects of special interest were analyzed using `SNID` in order to determine their astronomical type. Among these was ZTF20aatpoos, which we classified as a Type IIP SN about 10 days after peak (see Section 4.4). This classification represents our first success in searching for SNe in the HETDEX database, and motivates efforts for further discovery.

### 4.2. Template Fitting Via $\chi^2$

The $\chi^2_N$ value (Equation (5)) was computed for all 636 observed spectra using all templates in both the stellar and the galaxy libraries. We defined three groups of objects, named `star`, `galaxy`, and `low`, as the initial classification categories for the observed spectra. Spectra that were noise dominated and did not reach `s/n = 3` were moved into the `low` category. Sources that had lower $\chi^2_N$ values for fits to $z = 0$ stellar templates than fits to galaxies at $z > 0$ were classified as stars, and the remaining spectra were, at first, labeled as galaxies. In Figure 3 examples for a star (top panel) and a galaxy (bottom panel) spectrum are shown.

In the next step, all spectra were inspected visually, and peculiar objects were moved into additional categories. We identified broad-lined AGNs (category `agn`) in the `galaxy` group using the measured width of their emission features. Since many of these sources showed only a single broad line in the relatively narrow wavelength interval observed by HETDEX (3500–5500 Å), their redshifts, as derived from the best-fitting galaxy template may differ substantially from the true value. These objects are analyzed further in Section 4.5. Finally, spectra that did not resemble any other members in the above categories were moved to the `uncertain` category.

[20] https://www.wiserep.org/

It is an interesting question whether the results from our simple classification scheme have any correlation with the classifications performed by the ALeRCE pipeline. To test for this, we cross-compared our classification results for each transient (`star`, `galaxy`, `agn`, and `low`) to their most probable ALeRCE classification. From the various algorithms available in ALeRCE, we selected the one that had the highest probability value from the so-called "stamp classification" that uses the following categories: variable star (`VS`), AGN (`AGN`), SN (`SN`), asteroid (`AST`), and artifact (`BOGUS`). In addition, we introduced a sixth category, named unclassified (`UNC`), for those ZTF objects that were announced but had no ALeRCE classification available.

As an initial step, all sources belonging to the `BOGUS` category were rejected from the sample. Such "transients" usually appear in the vicinity of bright, saturated objects, e.g., near their diffraction spikes, and are artifacts of the ZTF image-subtraction process. A total of 251 such artifacts were removed from the sample, and only the remaining 385 spectra were analyzed further.

A summary of our cross-comparison can be found in Table 1 and is shown graphically in Figure 4. It is seen that the results from the $\chi^2$ template matching correlate very well with those from the ALeRCE stamp classification. For example, of the 149 sources with stellar-like HETDEX spectra, 114 were classified as `VS` by ALeRCE. Similarly, the 122 galaxy-like HETDEX spectra belong to ZTF transients that were classified by ALeRCE as either `AGN` or `SN`. It is especially encouraging that out of the 52 spectra that we classify as belonging to `AGN`, ALeRCE found 38 to be likely AGNs.

As expected, many of the low-S/N spectra, i.e., those that belong to the `low` category in our scheme, have no ALeRCE classification. It is also interesting that most of the transients that ALeRCE identified as most likely SNe are associated with either galaxies or noise-dominated sources. This is also an expected result, because many of the HETDEX spectra were taken outside the visibility window of an active transient, resulting in either a low-S/N spectrum or that of the likely host galaxy.

Although our HETDEX spectral extractions were all at the announced coordinates of the ZTF transients, many of the spectra are not actually associated with a transient object, due to the object's finite visibility window. In order to overcome this issue, we identified the "active" transients that were stamp classified as `SN` by ALeRCE and were observed by HETDEX when their ZTF follow up was still active. Nine such objects, collected in Table 2, were found. Their ZTF subframes, downloaded from the ALeRCE website, are shown in Figure 5, while their HETDEX spectra and the results of their $\chi^2$ classifications are plotted in Figure 6.

It is seen that three of the objects that were stamp classified as `SN` by ALeRCE (ZTF18aamlgvn, ZTF18aaqmidj, and ZTF18aaxqqxd) have low -S/N spectra that prevented a reliable classification. (In fact, the latter two appear to be artifacts from the same very bright star.) Of the remaining six objects, three are galaxies, one is a star and another is a broad-lined AGN. Of the set, ZTF19aceckmm is the most interesting, because it is located near a bright galaxy (see Figure 5), and has a ZTF light curve (shown on the ALeRCE website) that resembles that of a Type I SN. Unfortunately, the HETDEX spectrum was taken 141 days after the ZTF discovery, when the SN had already faded below the HETDEX detection limit.

The last object, ZTF20aatpoos, which we classified as `uncertain`, is the only object in the sample that shows

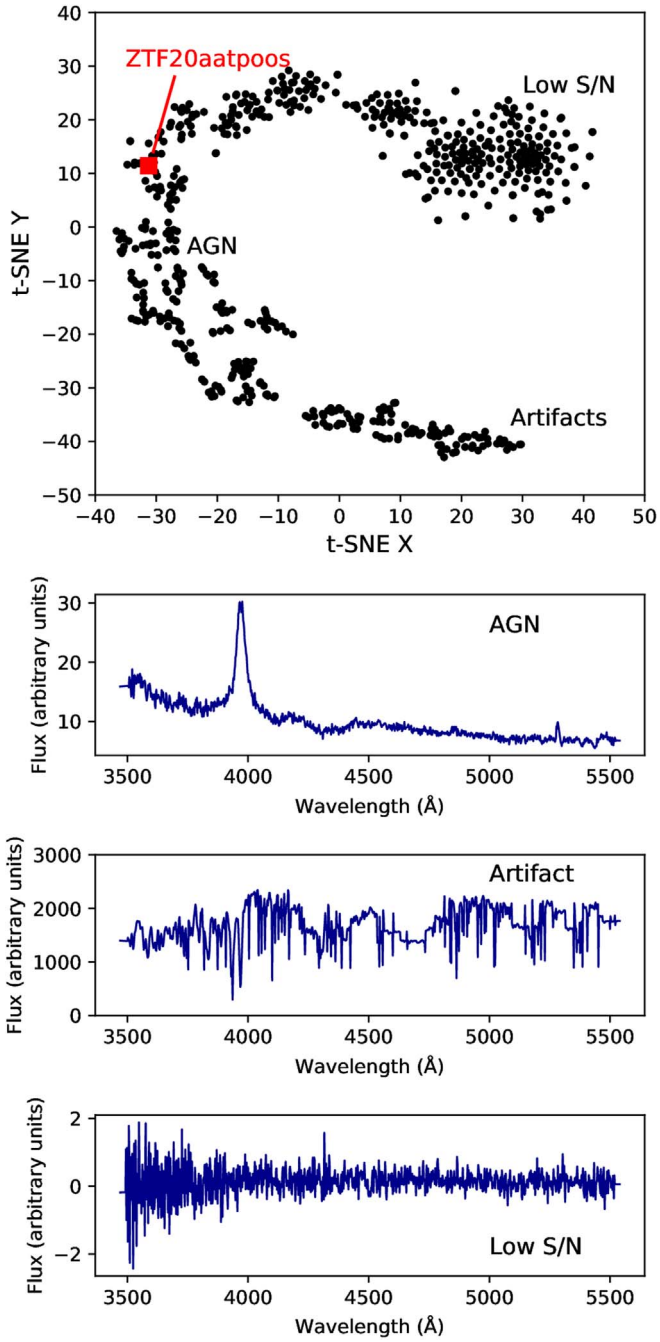


**Figure 2.** Top panel: the output embedding of our 636 HETDEX–ZTF spatially matched spectra from t-SNE. Each point represents an HETDEX spectrum, and spectra that are similar are clustered together. The classes that dominate each region of the map are marked in the text. ZTF20aatpoos is shown as a red square, and is found in a map region that is otherwise primarily inhabited by passive galaxies. Bottom panels: example spectra of an AGN, a pipeline artifact, and a low-S/N object are shown for the three categories marked on the top panel.

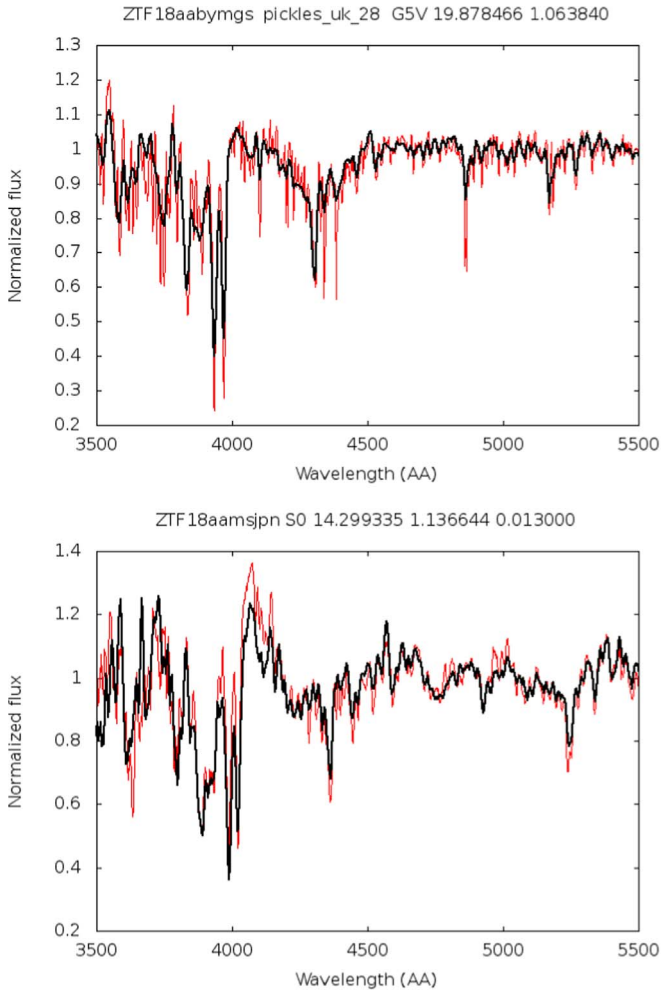


**Figure 3.** The continuum-normalized spectrum of a star (ZTF18abymgs) and a galaxy (ZTF18aamsjpn) plotted as red curves together with their best-fit normalized templates (black curves).

neither a stellar- nor a galaxy-like spectrum (see Figure 6). In fact, the spectrum is that of a Type IIP SN, which was also found as an SN candidate in Sections 4.1 and 4.3 below. More details on this object are presented in Section 4.4.

### 4.3. Cross-correlation

In the left panel of Figure 7, the peak height of the CCF is shown against the object indices of the HETDEX spectra. It is seen that for the majority of objects, the CCF is below 0.6, which we set as an initial threshold: each spectrum exceeding this threshold was inspected visually to check whether the similarity with the SN template was real.

In the right panel of Figure 7 the same quantity is plotted against the redshift provided by `fxcor`. This diagram is useful because objects with negative redshifts can immediately be rejected from the list of SN candidates, even though they may reach higher CCF peaks. As a first approximation, any object above the 0.6 threshold level *and* having positive redshift was considered a real candidate.

In both diagrams of Figure 7, the object that has the highest CCF peak (by far) is ZTF20aatpoos; this source was also identified as a good SN candidate in the previous sections. All other candidates having $z > 0$ and CCF $> 0.6$ turned out to be

**Table 1**
Statistics of the Classified Objects by Their ALeRCE Categories

| Sp. class | Total | VS | AGN | SN | AST | UNC |
|---|---|---|---|---|---|---|
| star | 149 | 114 | 18 | 6 | 0 | 11 |
| galaxy | 122 | 2 | 61 | 50 | 0 | 9 |
| agn | 52 | 4 | 38 | 7 | 0 | 3 |
| low | 64 | 0 | 6 | 30 | 4 | 32 |

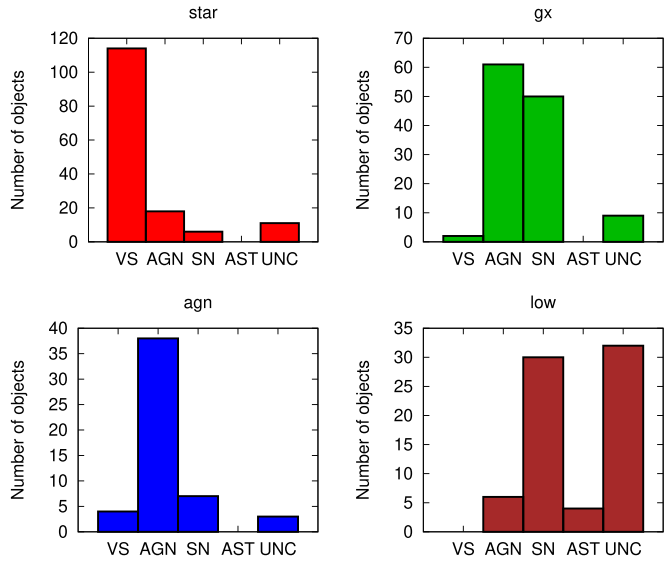


**Figure 4.** Sources classified via $\chi^2$ minimization as a function of their ALeRCE categories (VS, AGN, SN, AST, and UNC; see the main text). Each panel shows a histogram from sources belonging to the same HETDEX spectral type, namely stars (top left), galaxies (top right), AGNs (bottom left), and low-S/N objects (bottom right panel).

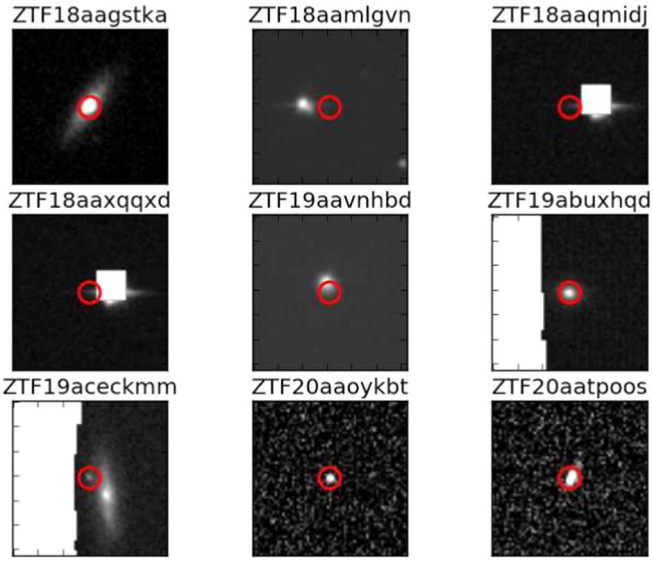


**Figure 5.** ZTF frame stamps (size $78'' \times 78''$) taken in the *r* band for the active ALeRCE SNe. North is up and east is to the left in each stamp. The white squares indicate masks placed onto saturated pixels.

**Table 2**
Active ZTF Transients Classified as SNe by ALeRCE

| Name | R.A. (deg) | Decl. (deg) | $MJD_{DEX}$ | $\Delta t$ (d) | AL type | AL prob. | Sp. type | S/N | $\chi^2$ | $z$ | Class. |
|---|---|---|---|---|---|---|---|---|---|---|---|
| ZTF18aagstka | 226.937577 | 51.452847 | 58660 | 405 | SN | 0.4370 | SB4 | 3.1275 | 0.2609 | 0.045 | galaxy |
| ZTF18aamlgvn | 230.134233 | 51.274517 | 58314 | 38 | SN | 0.4128 | ⋯ | 1.9978 | 2.3363 | 0 | low |
| ZTF18aaqmidj | 185.676093 | 51.375824 | 58495 | 195 | SN | 0.4317 | ⋯ | 0.001 | 0.001 | 0 | low |
| ZTF18aaxqqxd | 185.675409 | 51.375815 | 58495 | 223 | SN | 0.3498 | ⋯ | 3.0660 | 2.4245 | 0 | low |
| ZTF19aavnhbd | 267.924007 | 65.042444 | 58720 | 87 | SN | 0.4321 | G0V | 10.4723 | 1.1244 | 0 | star |
| ZTF19abuxhqd | 15.680562 | 0.720323 | 58788 | 62 | SN | 0.3881 | S0 | 13.9679 | 3.1949 | 0.080 | galaxy |
| ZTF19aceckmm | 172.320355 | 51.525159 | 58907 | 141 | SN | 0.7280 | SB6 | 7.4568 | 2.5238 | 0.032 | galaxy |
| ZTF20aaoykbt | 181.108375 | 55.606322 | 58952 | −2 | SN | 0.5260 | SB6 | 11.3571 | 3.1397 | 0.056 | agn |
| ZTF20aatpoos | 186.512456 | 55.702264 | 58954 | 18 | SN | 0.6277 | SB6 | 9.1188 | 2.1196 | 0.033 | uncertain |

**Note.** Columns: (1) ZTF name; (2), (3): J2000 coordinates in degrees; (4): MJD of the HETDEX observation; (5): time difference between the HETDEX observation and the beginning of the ZTF follow up in days; (6): most probable ALeRCE type; (7): ALeRCE classification probability; (8) spectral type of the best-matching template; (9): S/N parameter; (10): normalized $\chi^2$; (11): redshift; and (12): $\chi^2$ classification.

broad-line AGNs with strong emission lines, thus showing that their spectral overlap with the SN templates is artificial.

After the visual inspection of all HETDEX spectra of "real" (i.e., not BOGUS, see Section 3.2) sources, we also identified ZTF19abdkelq as a potential SN candidate. This spectrum was classified as low by the $\chi^2$ template-matching algorithm because of its low-s/n parameter, but the CCF method indicated some resemblance with the spectra of Type Ia SNe. In this case, the peak of the CCF is lower than the empirical threshold (0.6) due to the dominance of observational noise.

More details on these two SN candidates, ZTF20aatpoos and ZTF19abdkelq, are presented in the next subsection.

### 4.4. SNe

The strongest candidate for being an SN in our HETDEX sample is ZTF20aatpoos. This object was originally classified as an SN by ALeRCE, and announced on the Transient Name Server (TNS) website[21] as AT 2020fiz on 2020 March 29 (see Table 3). HETDEX observed this target serendipitously on 2020 April 15, ∼2 weeks after discovery.

ZTF20aatpoos was identified as an SN candidate by all of our SN finding methods. In Figure 8 we plot its observed spectrum (black curve) together with the best-matching SN templates: our SN template (red curve) is shown in the bottom left panel, while a template found by SNID is plotted with red on the right panel. It is seen that both CCF-based codes found approximately the same SN template—that for a relatively young (10–20 days after explosion) Type IIP SN.

ZTF20aatpoos was followed up by ZTF for 109 days after discovery, and its light curve (plotted in Figure 9) fully confirms that it shows the ∼100 day-long plateau, characteristic of Type IIP SNe. Template light curves from the data of the Type IIP SN 2005cs (Pastorello et al. 2009) in the *V* and *R* bands are shown for comparison.

We also computed a synthetic *g*-band AB magnitude for ZTF20aatpoos directly from the HETDEX spectrum. The value, $g = 19.180 \pm 0.002$ mag, is plotted as an orange square in Figure 9. It is seen that it agrees very well with the *g*-band ZTF photometry taken at similar epochs.

[21] https://www.wis-tns.org/

**Table 3**
Parameters of the SNe Found in HETDEX

| ZTF Name | IAU Name | R.A. (deg) | Decl. (deg) | Date | SNID Type | SNID $z$ | SNID Phase (day) |
|---|---|---|---|---|---|---|---|
| ZTF19abdkelq | ⋯ | 23.086249 | 0.658040 | 2019-08-08 | Ia | 0.125±0.011 | $40.4 \pm 20.1$ |
| ZTF20aatpoos | AT 2020fiz | 186.512456 | 55.702264 | 2020-04-15 | IIP | $0.026 \pm 0.013$ | $10.7 \pm 6.3$ |

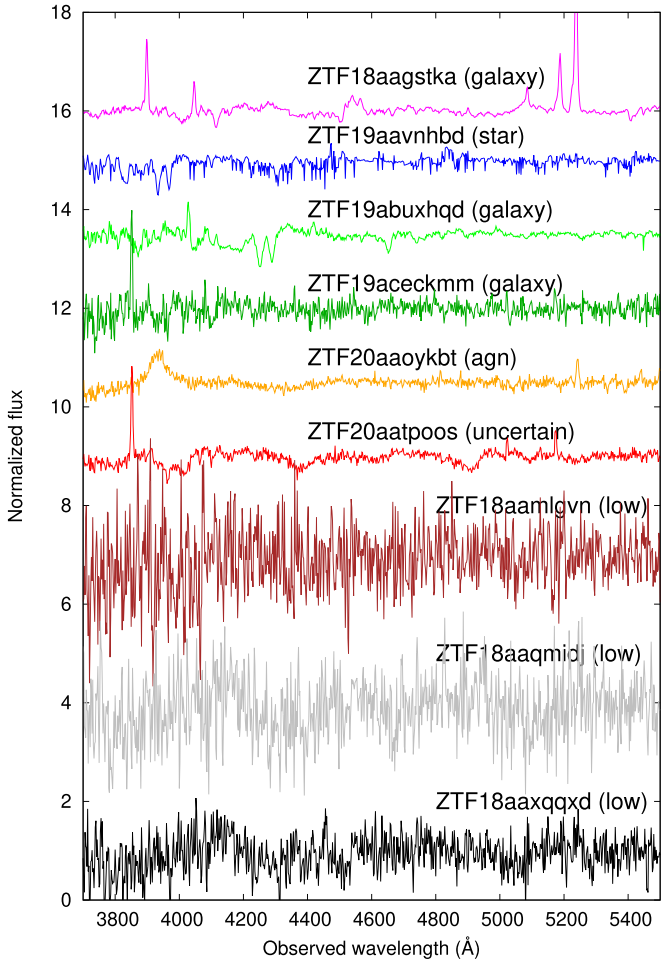


**Figure 6.** Normalized HETDEX spectra of the active transients classified as SNe by ALeRCE.

Our other SN candidate, ZTF19abdkelq, was originally classified as an asteroid (AST) by ALeRCE, but ZTF also recorded *r*-band magnitudes at four later epochs, with the last ZTF detection occurring ∼30 days after discovery. Thus, it is unlikely that this source is a moving object. Since it was not flagged as a transient, there is no available TNS record for the object.

The HETDEX spectrum of ZTF19abdkelq is plotted in Figure 10. In the left panel, we show the continuum-normalized spectrum (plotted with red) together with the best-matching Hsiao SN Ia template (black). Even though the observed spectrum is noisy, the pseudoemission feature around 5200 Å is a good match to the template spectrum. The resemblance is strengthened by the analysis with SNID (right panel), which suggests SN 2000cx, a peculiar Type Ia SN, as the best-matching template. Both our CCF code and SNID provided a consistent redshift for ZTF19abdkelq of $z \sim 0.12$.

In Figure 11, the light curve of ZTF19abdkelq is plotted from ZTF *r*-band photometry. The green and blue curves show the expected brightness decline of a Type Ia SN, as inferred from rest-frame *V*- and *B*-band template light curves from MLCS2k2 (Jha et al. 2007). At $z \sim 0.12$, the rest-frame *V*-band template light curve represents the observer-frame *r*-band data well. The result of *g*-band synthetic photometry from the HETDEX spectrum ($g = 22.144 \pm 0.098$ mag) is also shown as an orange square. It is seen that both the ZTF and the HETDEX photometry are entirely consistent with the proposed Type Ia SN classification of ZTF19abdkelq.

The parameters for the two SNe found in HETDEX are summarized in Table 3.

### 4.5. AGNs

Members of the AGN group were identified via the $\chi^2$ minimization method (see Section 3.2), although some were also found by cross-correlating the spectra with SN templates (Section 3.3). We identified 52 spectra (Table 1) that had a galaxy spectrum as their best-matching template, but also showed broader emission features than those of the star-forming galaxy templates. After visual inspection, three of them turned out to be saturated stars, which were then removed from the sample. The remaining 49 were analyzed further.

Redshifts were derived by fitting the "high luminosity QSO" template spectrum taken from the Sloan Digital Sky Survey (SDSS) site[22] to the AGN spectra. The fitting parameters for the AGN sample are collected in Table A2 in the Appendix.

Figure 12 shows the s/n parameter of each spectrum (see Section 3.2) against redshift. It is seen that most of the ZTF transients that turned out to be AGNs are at low redshifts, i.e., at $z \lesssim 0.5$. As a comparison, the full HETDEX AGN sample (Liu et al. 2022) extends to at least $z \sim 3.5$ and has a median redshift of $z_{\rm med} \sim 2.1$; in other words, the AGNs identified here are more local than the majority of the HETDEX AGNs. This is most likely due to the sensitivity limit of the ZTF public stream, which is $m_{\rm AB} \lesssim 20$ mag. This limit is significantly brighter than the HETDEX detection threshold for AGNs ($m_{\rm AB} \sim 26$ mag; Liu et al. 2022).

In Figure 13, spectra of some of the ZTF AGN sources are plotted against rest-frame wavelengths compared to the SDSS QSO template. One object, ZTF20aappepk ($z \sim 2.29$) has an HETDEX spectrum that extends beyond the blue edge of the SDSS QSO template, but the overlapping part shows good agreement with the template, just like the other, lower-redshifted AGNs in this small sample.

### 4.6. Host Galaxies of SNe

Information on the host galaxies of transients can be as important as the transients themselves. HETDEX presents a unique opportunity to gather spectra of transient host galaxies with a minimal observational cost: if an SN exploded within an

[22] https://classic.sdss.org/dr5/algorithms/spectemplates/

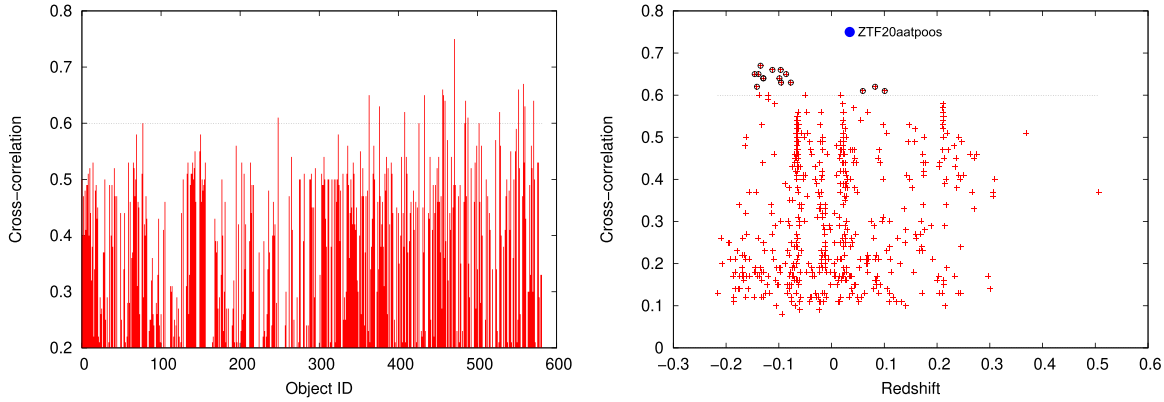


**Figure 7.** The maximum cross-correlation coefficient plotted against spectrum ID (left panel) and redshift (right panel) for the HETDEX sample. The dotted horizontal line marks the chosen threshold value for SN candidates (see text).

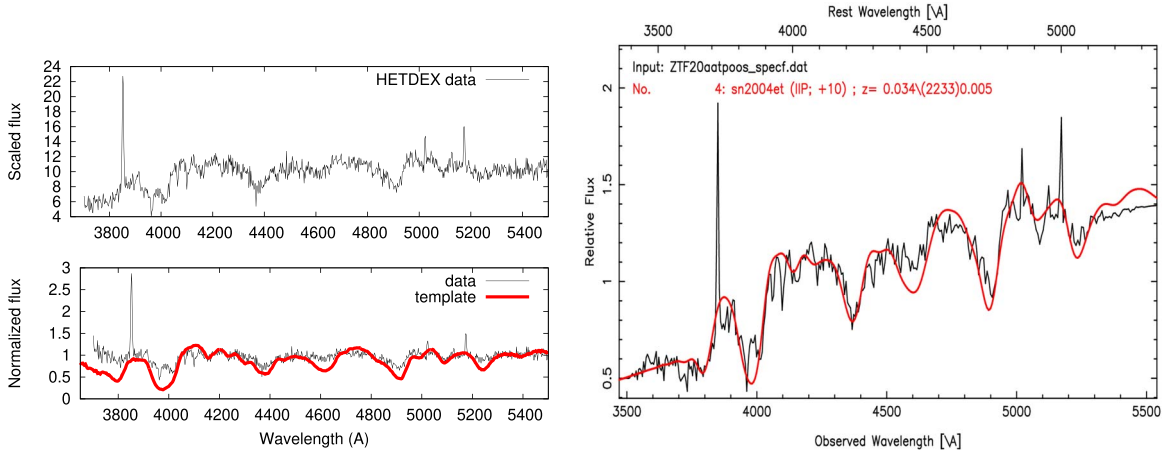


**Figure 8.** The spectrum of ZTF20aatpoos, a Type IIP SN at ∼10 days after explosion (plotted as a black curve), compared to a Type IIP SN template (red curve). The left panel shows the result from our cross-correlation analysis (see Section 4.3), while the right panel displays the output from `SNID`.

HETDEX field, then it should be possible to extract the host galaxy spectrum from the HETDEX data products. While such a dedicated study of transient host galaxies is beyond the scope of the present study, it may be a fruitful endeavor for future work.

Here we present galaxy types and redshifts for those HETDEX galaxies that were extracted at the position of ZTF transients that were classified as SNe by ALeRCE. We found 50 such objects according to Table 1, of which 21 had a refined ALeRCE SN classification based on their ZTF light curves. ALeRCE uses the following categories from its `lc_classification_transient` pipeline: `SNIa`, `SNIbc`, `SNII`, and `SLSN`. This subsample is listed in Table A3 in the Appendix, together with the host galaxy properties found by the $\chi^2$-classification method (Section 3.2).

The distribution of the host galaxy types for this subsample is shown in Figure 14. Here we added the numbers of `SNIbc` SNe to that of the `SNII` objects, and use the `SNcc` category for those core-collapse SNe. Note that the numbers for the `SLSN` category are probably overestimated by ALeRCE. The same distribution for the whole sample (i.e., with those objects that do not have an ALeRCE light-curve classification) is also plotted via the red bars. It is clear that even though the numbers are too low for any robust conclusions, most of the SNe occurred in starburst galaxies showing strong emission features. Since core-collapse SNe originating from massive stars likely dominate our low-redshift sample, the distribution of host galaxy types as shown in Figure 14 is consistent with expectations.

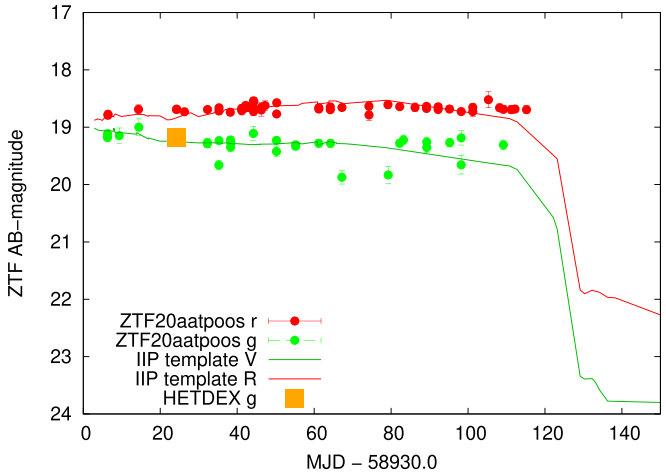


**Figure 9.** ZTF photometry of ZTF20aatpoos (*r* band: red dots; *g* band: green dots) compared to SN IIP template light curves, shifted vertically to match the observations. The *g*-band synthetic photometry from the HETDEX spectrum is plotted with an orange square.

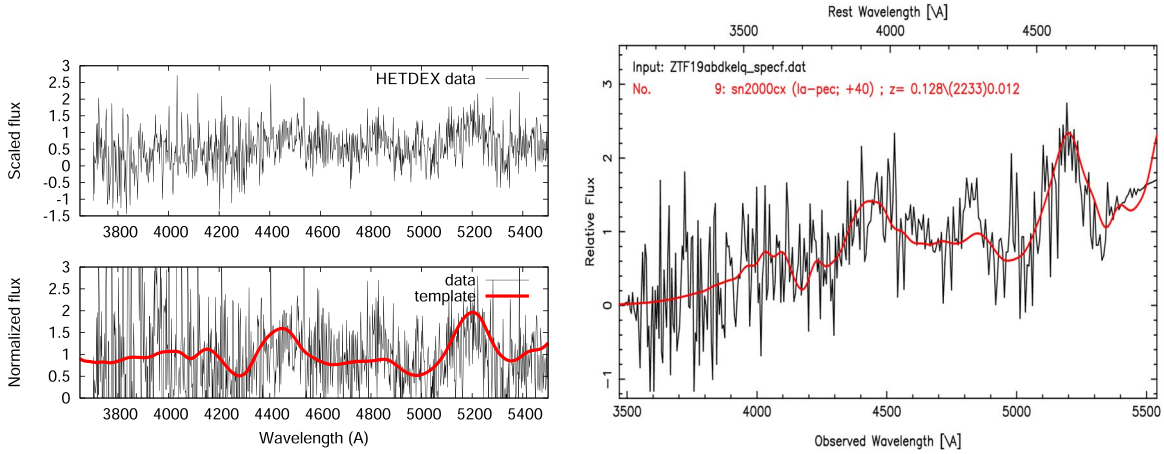


**Figure 10.** The same as Figure 8 but for the Type Ia SN ZTF19abdkelq, observed at ∼40 days after maximum light.

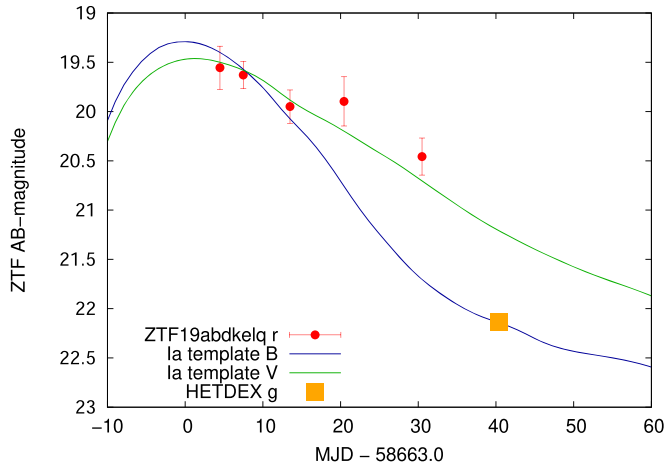


**Figure 11.** *r*-band ZTF photometry for ZTF19abdkelq, plotted together with Ia template light curves in rest-frame *B* and *V* bands. The *g*-band synthetic photometry from the HETDEX spectrum is shown by the orange square.

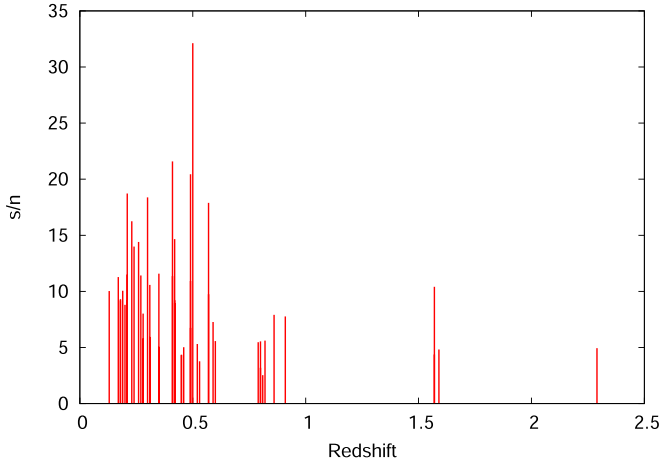


**Figure 12.** The `s/n` parameter of the AGN spectra as a function of redshift.

Note that ZTF19abuxhqd, which was classified as a likely Type II SN by ALeRCE, occurred in an early-type (S0) galaxy. This would be peculiar, since early-type galaxies usually host Type Ia SNe that originate from older populations of stars; however, a close inspection of the noise-dominated ZTF light curve of ZTF19abuxhqd provides no convincing evidence for the presence of a core-collapse SN. Specifically, the transient showed random-like brightness fluctuations for ∼400 days, instead of any sign of a decline.

The distribution of the redshifts for the whole sample, as well as for those SNe that have refined ALeRCE types, are plotted in Figure 15. This figure confirms that the ZTF SNe whose host galaxies could be measured by HETDEX are distributed in the $z < 0.3$ low-redshift space.

### *4.7. The Expected Number of SNe in HETDEX*

Even though HETDEX is not an ideal survey for finding extragalactic transients (see Section 1), the number of SNe that are expected to show up within the survey footprint may be of interest. Since the classification of new transients generally needs spectroscopy, the future HETDEX data releases could be useful for classifying targets that might otherwise escape attention.

The expected number of SNe within the survey area ($\Omega$) covered by observations during the survey time ($T_S$) in redshift interval $\Delta z$ at redshift $z$ can be expressed as,

$$N_{\rm SN}(z,\,\Delta z) = \Omega T_s \int_{z-\Delta z}^{z} \frac{R_{\rm SN}}{1+z}\frac{dV}{dz}dz, \qquad (7)$$

where $R_{\rm SN}$ is the measured SN volumetric rate (the number of SNe per Mpc$^3$ per year) and $dV/dz$ is the differential comoving volume. The factor $1+z$ accounts for cosmological time dilation.

The HETDEX survey field consists primarily of two parts: a spring field of 390 deg$^2$ and a fall field of 150 deg$^2$. Due to gaps between the IFUs, the effective survey field of view is ∼94 deg$^2$ (Gebhardt et al. 2021). The area covered by a single shot with VIRUS is ∼0.015 deg$^2$. To estimate the number of SNe found during a year, we assume that, on average, ∼three such fields are taken on each night in a year for either the spring or the fall fields. For the volumetric SN rates, we adopt $R_{\rm Ia} = 2.5\times10^{-5}\times(1+z)^{1.5}$ SNe Mpc$^{-3}$ yr$^{-1}$ for SNe Ia (Hounsell et al. 2018) and $R_{\rm CC}(z=0.028) = 9.1\times10^{-5}$ SNe Mpc$^{-3}$ yr$^{-1}$ for core-collapse SNe (Frohmaier et al. 2021). The latter is scaled with the cosmic star formation rate function by Hopkins & Beacom (2006) for different redshifts. Thus, using $\Omega = 3\times0.015 = 0.045$ deg$^2$, $T_s = 1$ year, and the volumetric SN rates given above, we get $N_{\rm Ia}\sim0.24$ SN Ia in the $0 < z < 0.3$ redshift range. Since core-collapse SNe are

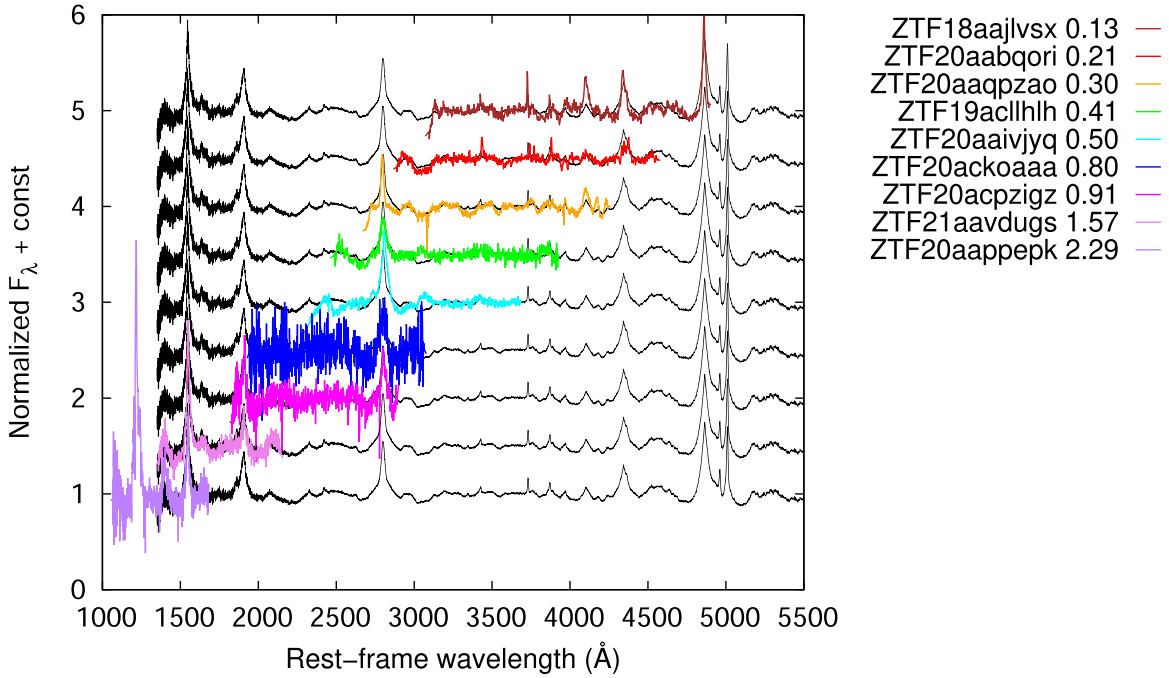


**Figure 13.** Observed spectra of a subsample of AGNs compared to the rest-frame SDSS QSO template.

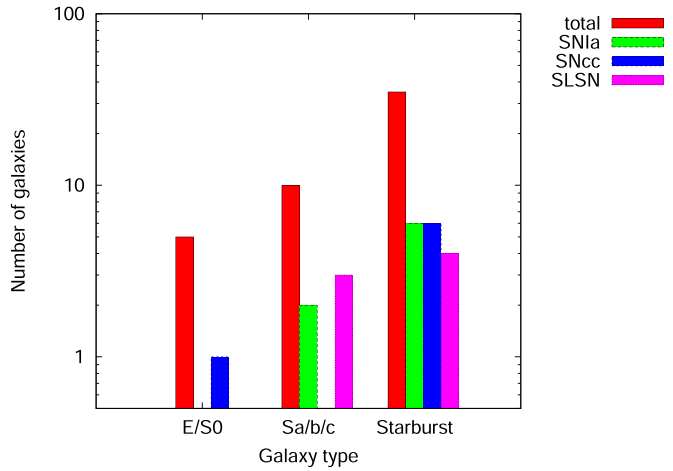


**Figure 14.** Distribution of host galaxy types for SNe with known light-curve classifications (green, blue, and magenta bars) as well as that of the whole sample (red bars).

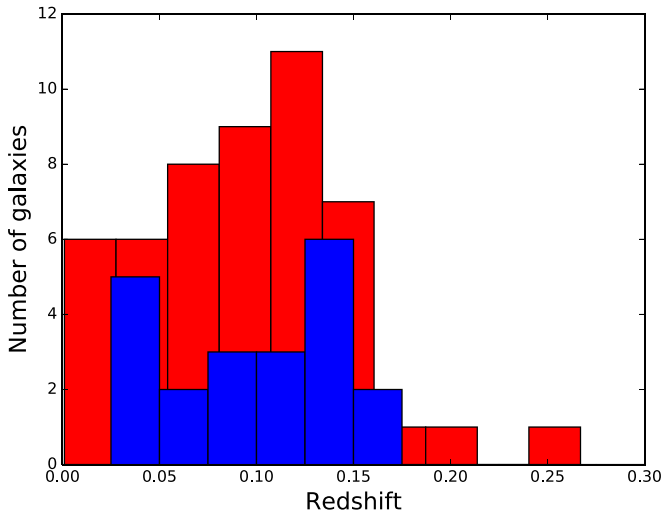


**Figure 15.** Histogram of host galaxy redshifts for the whole sample (red) and those having known ALeRCE light-curve classifications (blue).

fainter by $\lesssim$1 magnitude than Type Ia SNe, they are accessible by HETDEX only in the $0 < z < 0.2$ redshift range (assuming $\sim$22 mag as the detection limit of continuum sources in HETDEX). Within this volume we get $N_{CC} \sim 0.38$ core-collapse SN per year. This optimistic calculation does not take into account detection efficiencies (S/N, for example), thus, it is likely an overestimate, but the final numbers are consistent with our results (one SN of both types within $\sim$5 yr of HETDEX operation). Note that between 2017 and 2022 the HETDEX field of view was not completely filled up by IFUs, which decreased our chances to find transients. Starting from 2022, having the field of view fully populated by 78 IFUs, the probability of discoveries are expected to increase. Overall, we conclude that we can expect to find a few more ($N \lesssim 5$) SNe during the upcoming years of HETDEX operation.

## 5. Conclusions

The conclusions of the present study are summarized as follows:

1. We identified the counterparts of 583 transient objects in the HETDEX spectral database (but not necessarily at the same epoch) out of 4845 transient sources found by ALeRCe in the ZTF public data stream. In total, 636 spectra covering the 3500–5500 Å wavelength range were extracted from the HETDEX observing archive and analyzed.
2. We applied the t-SNE ML method to explore the data set and identify potentially interesting sources. Our primary intention was to identify SNe, which succeeded in two cases (see below).

3. All ZTF sources having HETDEX spectra were classified into the `star`, `galaxy`, `agn`, and `low` categories based on matching with template spectra (or, in the last case, having low S/Ns). For most objects, these categories agreed very well with their "stamp classification" made by the ALeRCe pipeline for their ZTF counterparts.
4. We attempted to find SNe among the HETDEX spectra in three different ways: visual inspection of the t-SNE 2D output, looking for outliers in the $\chi^2$ template-matching classification, and cross-correlation with SN templates. ZTF20aatpoos was flagged by all three methods as a potential SN, which was successfully confirmed as a Type IIP event using `SNID`. We also identified another SN candidate, ZTF19abdkelq, among the low -S/N sources, and `SNID` confirmed it to be a Type Ia SN taken $\sim$40 days after maximum light.
5. As a by-product, we identified 49 AGN sources, most of them at low ($z \lesssim 0.5$) redshifts; 38 of these were also classified as AGNs by ALeRCe.
6. We obtained host galaxy spectra for 50 ZTF transients classified as SNe by ALeRCE. Most turned out to be starburst galaxies, which is consistent with the expectation that core-collapse events dominate the SN sample in the low-redshift ($z \lesssim 0.3$) universe.

We expect to find a few ($\lesssim$5) more SNe during the upcoming years of the HETDEX survey.

HETDEX is led by the University of Texas at Austin McDonald Observatory and Department of Astronomy with participation from the Ludwig-Maximilians Universitat Munchen, Max-Planck-Institut fur Extraterrestrische Physik (MPE), Leibniz-Institut fur Astrophysik Potsdam (AIP), Texas A&M University, The Pennsylvania State University, Institut fur Astrophysik Gottingen, the University of Oxford, Max-Planck Institut fur Astrophysik (MPA), the University of Tokyo, and Missouri University of Science and Technology. In addition to institutional support, HETDEX is funded by the National Science Foundation (grant AST0926815), the State of Texas, the US Air Force (AFRL FA9451-04-2-0355), and generous support from private individuals and foundations.

The Hobby–Eberly Telescope (HET) is a joint project of the University of Texas at Austin, the Pennsylvania State University, Ludwig-Maximilians-Universitat Munchen, and Georg-August-Universitat Gottingen. The HET is named in honor of its principal benefactors, William P. Hobby and Robert E. Eberly.

VIRUS is a joint project of the University of Texas at Austin, Leibniz-Institut für Astrophysik Potsdam (AIP), Texas A&M University (TAMU), Max-Planck-Institut für Extraterrestriche-Physik (MPE), Ludwig-Maximilians-Universität München, Pennsylvania State University, Institut für Astrophysik Göttingen, University of Oxford, and the Max-Planck-Institut für Astrophysik (MPA).

The authors acknowledge the Texas Advanced Computing Center (TACC) at The University of Texas at Austin for providing high-performance computing, visualization, and storage resources that have contributed to the research results reported within this paper. URL:http://www.tacc.utexas.edu.

The University of Texas at Austin sits on indigenous land. The Tonkawa lived in central Texas and the Comanche and Apache moved through this area. The Davis Mountains that host McDonald Observatory were originally husbanded by Lipan Apache, Warm Springs Apache, Mescalero Apache, Comanche, and various tribes of the Jumanos. We acknowledge and pay our respects to all the Indigenous Peoples and communities who are or have been a part of these lands and territories in Texas.

J.V., B.P.T., and J.C.W. are supported by NSF grant AST1813825.

Z.J. was supported by a PRODEX Experiment Agreement No. 4000137122 between the ELTE Eötvös Loránd University and the European Space Agency (ESA-D/SCI-LE-2021-0025).

The Institute for Gravitation and the Cosmos is supported by the Eberly College of Science and the Office of the Senior Vice President for Research at the Pennsylvania State University.

An anonymous referee provided useful comments and suggestions that are acknowledged with gratitude.

*Facilities:* Hobby–Eberly Telescope (HET); Zwicky Transient Facility (ZTF); Texas Advanced Computing Center (TACC).

*Software:* `ALeRCE`: http://alerce.science/; `IRAF`: https://iraf-community.github.io/ (Tody 1986, 1993); `Astropy`: http://www.astropy.org (Astropy Collaboration et al. 2013, 2018); `numpy`: https://numpy.org (Harris et al. 2020); `scipy`: https://scipy.org (Virtanen et al. 2020); `matplotlib`: https://matplotlib.org (Hunter 2007); `scikit-learn`: https://scikit-learn.org/stable/ (Pedregosa et al. 2011); `pandas`: https://pandas.pydata.org/ (McKinney 2010); `SNID`: https://people.lam.fr/blondin.stephane/software/snid/index.html (Blondin & Tonry 2007).

## Appendix

Table A1 lists the parameters of the ZTF transients classified via $\chi^2$ minimization (Section 3.2). Only a few objects are given here to illustrate the data structure. The full table in electronic form can be accessed on GitHub[23] or in a machine-readable format in the online Journal.

Table A2 shows the fitting parameters (S/N, $\chi^2$ and redshift) for the AGNs. Table A3 gives the same parameters, plus the ALeRCE SN type, the SN classification probability and the fitted galaxy spectral type for the SN host galaxies,

[23] https://github.com/jozsefvinko/Transients-in-HETDEX

**Table A1**
ZTF Transients Classified Via $\chi^2$ minimization

| Name | R.A. (deg) | Decl. (deg) | $MJD_{start}$ | $MJD_{stop}$ | $MJD_{DEX}$ | AL type | AL prob. | Sp. type | S/N | $\chi^2$ | z | Class. |
|---|---|---|---|---|---|---|---|---|---|---|---|---|
| ZTF17aaclhdu | 33.36269135 | −0.87615907 | 58781.3 | 59079.5 | 58862 | AGN | 0.46 | G0V | 16.44 | 0.9381 | 0 | star |
| ZTF18aagstka | 226.93757719 | 51.45284761 | 58255.3 | 59641.4 | 58660 | SN | 0.43 | SB4 | 3.12 | 0.2609 | 0.045 | galaxy |
| ZTF18aaguppa | 230.02485526 | 51.14954140 | 59067.2 | 59094.2 | 58173 | ⋯ | ⋯ | M2V | 0.96 | 1.3199 | 0 | low |
| ZTF18aaiwfgo | 197.17922553 | 55.52398578 | 59291.3 | 59316.3 | 58958 | AGN | 0.65 | Sa | 8.02 | 1.9890 | 0.079 | agn |
| ⋮ | ⋮ | ⋮ | ⋮ | ⋮ | ⋮ | ⋮ | ⋮ | ⋮ | ⋮ | ⋮ | ⋮ | ⋮ |

(This table is available in its entirety in machine-readable form.)

**Table A2**
Parameters of the AGN Sample

| ZTF name | S/N | $\chi^2$ | $z$ | ZTF name | S/N | $\chi^2$ | $z$ |
|---|---|---|---|---|---|---|---|
| ZTF18aaiwfgo | 8.01 | 1.2152 | 0.28 | ZTF20aarsdui | 4.37 | 8.0946 | 1.57 |
| ZTF18aajlvsx | 10.02 | 0.6340 | 0.13 | ZTF20aasjgqr | 5.47 | 0.9711 | 0.79 |
| ZTF18aakqshm | 16.24 | 1.2993 | 0.23 | ZTF20aaxalny | 11.57 | 0.9945 | 0.35 |
| ZTF18aaktpmg | 9.21 | 11.2259 | 0.42 | ZTF20abakioq | 4.31 | 2.0508 | 0.45 |
| ZTF18aaqkxzg | 10.05 | 0.4965 | 0.19 | ZTF20abbfimy | 4.82 | 2.3148 | 1.59 |
| ZTF18aaxqtbj | 13.99 | 1.2383 | 0.24 | ZTF20abcamux | 9.19 | 0.4522 | 0.18 |
| ZTF18aceyycp | 9.22 | 0.6280 | 0.21 | ZTF20abcjsvg | 2.53 | 0.3731 | 0.81 |
| ZTF19aalbcut | 14.66 | 4.4769 | 0.42 | ZTF20abrigbg | 5.05 | 0.6352 | 0.35 |
| ZTF19aarioyj | 11.27 | 1.3345 | 0.17 | ZTF20abwfqoj | 9.74 | 5.6799 | 0.57 |
| ZTF19aasbotx | 11.42 | 1.2587 | 0.27 | ZTF20abxpvdk | 5.57 | 1.7046 | 0.60 |
| ZTF19aasccum | 5.30 | 2.6832 | 0.52 | ZTF20abxrxbh | 17.89 | 3.9041 | 0.57 |
| ZTF19acllhlh | 21.58 | 1.6776 | 0.41 | ZTF20ackoaaa | 5.54 | 0.9043 | 0.80 |
| ZTF20aabqori | 18.72 | 1.0551 | 0.21 | ZTF20acpzigz | 7.76 | 0.7796 | 0.91 |
| ZTF20aadbtju | 10.57 | 1.6565 | 0.31 | ZTF20acxtdub | 11.50 | 1.5784 | 0.21 |
| ZTF20aahgivv | 8.96 | 1.5503 | 0.42 | ZTF21aandbyi | 4.36 | 2.0195 | 0.45 |
| ZTF20aaicqat | 5.61 | 1.0932 | 0.82 | ZTF21aaplbpm | 5.02 | 3.9342 | 0.46 |
| ZTF20aaivjyq | 32.11 | 6.4454 | 0.50 | ZTF21aavdhbj | 3.18 | 1.8110 | 0.80 |
| ZTF20aajbuhw | 5.79 | 0.9001 | 0.28 | ZTF21aavdugs | 10.41 | 1.1423 | 1.57 |
| ZTF20aajcmsc | 9.30 | 0.4392 | 0.18 | ZTF21aayehok | 6.74 | 3.4700 | 0.49 |
| ZTF20aaliybg | 14.40 | 1.7369 | 0.26 | ZTF21aazcpmg | 3.77 | 2.0711 | 0.53 |
| ZTF20aankago | 7.90 | 0.9189 | 0.86 | ZTF21aazrcye | 5.93 | 0.8802 | 0.31 |
| ZTF20aaoyjbk | 10.92 | 1.9170 | 0.49 | ZTF21aazxsci | 8.80 | 1.2792 | 0.20 |
| ZTF20aaoykbt | 11.35 | 1.6181 | 0.41 | ZTF21abatxlh | 7.27 | 3.7249 | 0.59 |
| ZTF20aappepk | 4.93 | 2.3970 | 2.29 | ZTF21abiimfm | 20.44 | 2.4730 | 0.49 |
| ZTF20aaqpzao | 18.37 | 1.2529 | 0.30 | | | | |

(This table is available in machine-readable form.)

**Table A3**
Parameters of the Host Galaxies with an ALeRCE SN Light-curve Classification

| Name | SN Type | SN Type prob. | Host Type | S/N | $\chi^2$ | z |
|---|---|---|---|---|---|---|
| ZTF18aagstka | SN II | 0.408 | SB4 | 3.12 | 0.2609 | 0.045 |
| ZTF18aamsecj | SN II | 0.296 | SB6 | 9.27 | 2.3834 | 0.080 |
| ZTF18aaovsji | SLSN | 0.320 | SB1 | 6.96 | 6.8908 | 0.131 |
| ZTF18abkiqna | SN Ia | 0.330 | SB4 | 5.10 | 4.3505 | 0.130 |
| ZTF18abuatfp | SN II | 0.342 | SB6 | 11.81 | 5.3940 | 0.136 |
| ZTF18acwtrfe | SN Ibc | 0.336 | SB3 | 4.64 | 1.0119 | 0.049 |
| ZTF18acwyxnp | SLSN | 0.364 | Sa | 12.32 | 3.3459 | 0.130 |
| ZTF19aangier | SN Ia | 0.472 | Sb | 14.44 | 2.5332 | 0.060 |
| ZTF19abuxhqd | SN II | 0.346 | S0 | 13.96 | 3.1949 | 0.080 |
| ZTF19aceckmm | SN II | 0.462 | SB6 | 7.45 | 2.5238 | 0.032 |
| ZTF19acfxbki | SN Ia | 0.596 | Sa | 21.03 | 2.3064 | 0.058 |
| ZTF20aafcheh | SLSN | 0.418 | Sa | 12.44 | 3.3433 | 0.130 |
| ZTF20aagnbdf | SLSN | 0.438 | SB3 | 5.86 | 3.0425 | 0.089 |
| ZTF20aahhvci | SN Ia | 0.382 | SB3 | 4.32 | 2.0259 | 0.104 |
| ZTF20aaolglj | SLSN | 0.360 | SB3 | 9.39 | 1.6336 | 0.029 |
| ZTF20aausyrp | SN Ia | 0.296 | SB6 | 5.10 | 3.3010 | 0.026 |
| ZTF20aayxapt | SLSN | 0.376 | SB1 | 8.35 | 4.8623 | 0.145 |
| ZTF20abeiqzy | SLSN | 0.344 | Sa | 9.53 | 2.4443 | 0.171 |
| ZTF21aaoblpm | SN Ia | 0.384 | SB3 | 12.35 | 13.0117 | 0.117 |
| ZTF21aaplbom | SN Ibc | 0.360 | SB3 | 11.24 | 6.0530 | 0.121 |
| ZTF21abfjcap | SN Ia | 0.388 | SB6 | 12.76 | 3.6394 | 0.151 |

(This table is available in machine-readable form.)

## ORCID iDs


József Vinkó https://orcid.org/0000-0001-8764-7832
Benjamin P. Thomas https://orcid.org/0000-0002-0977-1974
J. Craig Wheeler https://orcid.org/0000-0003-1349-6538
Anna Y. Q. Ho https://orcid.org/0000-0002-9017-3567
Erin Mentuch Cooper https://orcid.org/0000-0002-2307-0146
Karl Gebhardt https://orcid.org/0000-0002-8433-8185
Robin Ciardullo https://orcid.org/0000-0002-1328-0211
Daniel J. Farrow https://orcid.org/0000-0003-2575-0652
Gary J. Hill https://orcid.org/0000-0001-6717-7685
Wolfram Kollatschny https://orcid.org/0000-0002-0417-1494
Chenxu Liu https://orcid.org/0000-0001-5561-2010
Enikő Regős https://orcid.org/0000-0002-9498-4957
Krisztián Sárneczky https://orcid.org/0000-0003-0926-3950


## References


Astropy Collaboration, Price-Whelan, A. M., Sipőcz, B. M., et al. 2018, AJ, 156, 123
Astropy Collaboration, Robitaille, T. P., Tollerud, E. J., et al. 2013, A&A, 558, A33
Bellm, E. C., Kulkarni, S. R., Graham, M. J., et al. 2019, PASP, 131, 018002
Bernstein, J. P., Kessler, R., Kuhlmann, S., et al. 2012, ApJ, 753, 152
Blondin, S., & Tonry, J. L. 2007, ApJ, 666, 1024
Carrasco-Davis, R., Reyes, E., Valenzuela, C., et al. 2021, AJ, 162, 231
Davis, D., Gebhardt, K., Mentuch Cooper, E., et al. 2021, ApJ, 920, 122
Dekany, R., Smith, R. M., Riddle, R., et al. 2020, PASP, 132, 038001
Donnan, C. T., McLeod, D. J., Dunlop, J. S., et al. 2023, MNRAS, 518, 6011
Elmhamdi, A., Danziger, I. J., Chugai, N., et al. 2003, MNRAS, 338, 939
Förster, F., Cabrera-Vives, G., Castillo-Navarrete, E., et al. 2021, AJ, 161, 242
Fremling, C., Miller, A. A., Sharma, Y., et al. 2020, ApJ , 895, 32
Frohmaier, C., Angus, C. R., Vincenzi, M., et al. 2021, MNRAS, 500, 5142
Gal-Yam, A. 2019, ARA&A, 57, 305
Gebhardt, K., Mentuch Cooper, E., Ciardullo, R., et al. 2021, ApJ, 923, 217
Gezari, S. 2021, ARA&A, 59, 21
Graham, M. J., Kulkarni, S. R., Bellm, E. C., et al. 2019, PASP, 131, 078001
Hamuy, M., Pinto, P. A., Maza, J., et al. 2001, ApJ, 558, 615
Harris, C. R., Millman, K. J., van der Walt, S. J., et al. 2020, Natur, 585, 357
Hawkins, K., Zeimann, G., Sneden, C., et al. 2021, ApJ, 911, 108
Hill, G. J., Lee, H., MacQueen, P. J., et al. 2021, AJ, 162, 298
Hopkins, A. M., & Beacom, J. F. 2006, ApJ, 651, 142
Hounsell, R., Scolnic, D., Foley, R. J., et al. 2018, ApJ, 867, 23
Hsiao, E. Y., Conley, A., Howell, D. A., et al. 2007, ApJ, 663, 1187
Hunter, J. D. 2007, CSE, 9, 90
Indahl, B., Zeimann, G., Hill, G. J., et al. 2021, ApJ, 916, 11
Ishida, E. E. O., Beck, R., González-Gaitán, S., et al. 2019, MNRAS, 483, 2
Ivezić, Ž., Kahn, S. M., Tyson, J. A., et al. 2019, ApJ, 873, 111
Jha, S., Riess, A. G., & Kirshner, R. P. 2007, ApJ, 659, 122
Kessler, R., Marriner, J., Childress, M., et al. 2015, AJ, 150, 172
Kinney, A. L., Calzetti, D., Bohlin, R. C., et al. 1996, ApJ, 467, 38
Liu, C., Gebhardt, K., Mentuch Cooper, E., et al. 2022, arXiv:2204.13658
Lujan Niemeyer, M., Komatsu, E., Byrohl, C., et al. 2022, ApJ, 929, 90
Masci, F. J., Laher, R. R., Rusholme, B., et al. 2019, PASP, 131, 018003
McKinney, W. 2010, in Proc. of the IX Python in Science Conf., ed. Stéfan van der Walt & Jarrod Millman (Trieste: SISSA), 56
Mentuch Cooper, E., Gebhardt, K., Davis, D., et al. 2023, arXiv:2301.01826
Pastorello, A., Valenti, S., Zampieri, L., et al. 2009, MNRAS, 394, 2266
Pedregosa, F., Varoquaux, G., Gramfort, A., et al. 2011, J. Mach. Learn. Res., 12, 2825
Perlmutter, S., Aldering, G., Goldhaber, G., et al. 1999, ApJ, 517, 565
Pickles, A. J. 1998, PASP, 110, 863
Press, W. H., Teukolsky, S. A., Vetterling, W. T., & Flannery, B. P. 2002, Numerical Recipes in C++ : The Art of Scientific Computing (Cambridge: Cambridge Univ. Press)
Ramsey, L. W., Adams, M. T., Barnes, T. G., et al. 1998, Proc. SPIE, 3352, 34
Regős, E., & Vinkó, J. 2019, ApJ, 874, 158
Regős, E., Vinkó, J., & Stermeczky, Z. V. 2021, ApJ, 909, 64
Regős, E., Vinkó, J., & Ziegler, B. L. 2020, ApJ, 894, 94
Riess, A. G., Filippenko, A. V., Challis, P., et al. 1998, AJ, 116, 1009
Tody, D. 1986, Proc. SPIE, 627, 733
Tody, D. 1993, in ASP Conf. Ser. 52, Astronomical Data Analysis Software and Systems II, ed. R. J. Hanisch, R. J. V. Brissenden, & J. Barnes (San Francisco, CA: ASP), 173
van der Maaten, L., & Hinton, G. 2008, J. Mach. Learn. Res., 9, 2579
Virtanen, P., Gommers, R., Oliphant, T. E., et al. 2020, NatMe, 17, 261
Zhang, Y., Ouchi, M., Gebhardt, K., et al. 2021, ApJ, 922, 167